JOURNAL OF VIROLOGY, Feb. 2011, p. 1214–1223 Vol. 85, No. 3
0022-538X/11/$12.00 doi:10.1128/JVI.01848-10


# Pandemic Swine-Origin H1N1 Influenza A Virus Isolates Show Heterogeneous Virulence in Macaques▽‡

David Safronetz,[1]† Barry Rockx,[1]† Friederike Feldmann,[1]† Sarah E. Belisle,[4,5]† Robert E. Palermo,[4,5] Douglas Brining,[2] Don Gardner,[2] Sean C. Proll,[4,5] Andrea Marzi,[1] Yoshimi Tsuda,[1] Rachel A. LaCasse,[2] Lisa Kercher,[2] Anthony York,[1] Marcus J. Korth,[4,5] Dan Long,[2] Rebecca Rosenke,[2] W. Lesley Shupert,[1] Celia Alpuche Aranda,[6] John S. Mattoon,[7] Darwyn Kobasa,[8] Gary Kobinger,[8] Yan Li,[8] Jeffery K. Taubenberger,[3] Jürgen A. Richt,[9] Michael Parnell,[2] Hideki Ebihara,[1] Yoshihiro Kawaoka,[10,11,12,13] Michael G. Katze,[4,5]* and Heinz Feldmann[1]*

*Laboratory of Virology (Hamilton, Montana),[1] Rocky Mountain Veterinary Branch (Hamilton, Montana),[2] and Laboratory of Infectious Diseases (Bethesda, Maryland),[3] Division of Intramural Research, National Institute of Allergy and Infectious Diseases, National Institutes of Health, Bethesda, Maryland; Department of Microbiology, School of Medicine,[4] and Washington National Primate Research Center,[5] University of Washington, Seattle, Washington; Instituto de Diagnóstico y Referencia Epidemiológicos, Prolongación de Carpio No. 470, 3er Piso, Col. Santo Tomas, Delegación Muguel Hidalgo, Mexico City, CP 11340, Mexico[6]; Department of Veterinary Clinical Sciences, Washington State University, Pullman, Washington[7]; National Microbiology Laboratory, Public Health Agency of Canada, Winnipeg, Manitoba, Canada[8]; Department of Diagnostic Medicine and Pathobiology, College of Veterinary Medicine, Kansas State University, Manhattan, Kansas[9]; Division of Virology, Department of Microbiology and Immunology, Institute of Medical Science, University of Tokyo, Tokyo 108-8639, Japan[10]; Influenza Research Institute, Department of Pathobiological Sciences, School of Veterinary Medicine, University of Wisconsin-Madison, Madison, Wisconsin[11]; ERATO Infection-Induced Host Responses Project, Saitama 332-0012 Japan[12]; and Creative Research Initiative, Sousei, Hokkaido University, Sapporo 060-0818, Japan[13]*

Received 31 August 2010/Accepted 5 November 2010

**The first influenza pandemic of the new millennium was caused by a newly emerged swine-origin influenza virus (SOIV) (H1N1). This new virus is characterized by a previously unknown constellation of gene segments derived from North American and Eurasian swine lineages and the absence of common markers predictive of human adaptation. Overall, human infections appeared to be mild, but an alarming number of young individuals presented with symptoms atypical for seasonal influenza. The new SOIV also showed a sustained human-to-human transmissibility and higher reproduction ratio than common seasonal viruses, altogether indicating a higher pathogenic potential for this newly emerged virus. To study the virulence of the SOIV, we used a recently established cynomolgus macaque model and compared parameters of clinical disease, virology, host responses, and pathology/histopathology with a current seasonal H1N1 virus. We here show that infection of macaques with two genetically similar but clinically distinct SOIV isolates from the early stage of the pandemic (A/Mexico/4108/2009 and A/Mexico/InDRE4487/2009) resulted in upper and lower respiratory tract infections and clinical disease ranging from mild to severe pneumonia that was clearly advanced over the mild infection caused by A/Kawasaki/UTK-4/2009, a current seasonal strain. Unexpectedly, we observed heterogeneity among the two SOIV isolates in virus replication, host transcriptional and cytokine responses, and disease progression, demonstrating a higher pathogenic potential for A/Mexico/InDRE4487/2009. Differences in virulence may explain more severe disease, as was seen with certain individuals infected with the emerged pandemic influenza virus. Thus, the nonhuman primate model closely mimics influenza in humans.**

A newly emerged swine-origin influenza virus (SOIV) (H1N1) caused the first influenza pandemic of the 21st century (1, 9). Sequence comparison revealed a unique virus with gene segments derived from North American and Eurasian swine lineages and the absence of any known markers predictive of human adaptation (10, 36), with the exception of a second-site suppressor mutation in PB2 (23). In general, human SOIV infections appear to be mild; however, some infected individuals presented with symptoms atypical for seasonal influenza, and more severe illness has been reported in young, previously healthy individuals (6, 11, 28, 30). This suggests that the new pandemic H1N1 virus is distinct from common seasonal influenza viruses. However, the actual pathogenic potential of the circulating virus pool remains unknown.

The pathogenic potential of human influenza viruses is often studied in mice and ferrets, although human H1N1 influenza viruses normally replicate efficiently in mice only after adaptation (13). In contrast, the SOIV isolates replicate efficiently in mouse lung and some isolates produce severe and even lethal infection under high-dose application (17, 22). Ferrets

* Corresponding author. Mailing address for H. Feldmann: Rocky Mountain Laboratories, 903 South 4th Street, Hamilton, MT 59840. Phone: (406) 375-7410. Fax: (406) 375-7416. E-mail: feldmannh@niaid.nih.gov. Mailing address for M. G. Katze: University of Washington, Department of Microbiology, Seattle, WA 98195-8070. Phone: (206) 732-6135. Fax: (206) 732-6056. E-mail: honey@u.washington.edu.
† D.S., B.R., F.F., and S.E.B. contributed equally to this study.
‡ Supplemental material for this article may be found at http://jvi.asm.org/.
▽ Published ahead of print on 17 November 2010.

are highly susceptible to infection with human influenza viruses and appear to better recapitulate human disease severity and transmissibility than mouse models (22, 24). As with mice, SOIV isolates replicate more efficiently in ferrets compared to currently circulating H1N1 isolates. However, higher transmissibility of SOIV in ferrets could not be conclusively demonstrated (17, 20, 22, 24).

Nonhuman primate models have been less extensively used in influenza research but are often thought to best impersonate human infectious diseases. In general, human influenza A viruses infect and replicate in the upper respiratory tract of macaques, causing either asymptomatic or mild clinical infections in these animals (2, 3). The exceptions are avian H5N1 (5, 31) and the 1918 H1N1 virus (18), the latter of which causes a severe/lethal acute respiratory distress syndrome (ARDS) in cynomolgus macaques that required euthanasia of the animals (18). Thus far, only two published studies have investigated the pathogenic potential of the newly emerged H1N1 pandemic virus in macaques (16, 17). In both studies, a single isolate (A/California/04/2009 [12, 17] or A/Netherlands/602/2009 [16]) showed efficient replication in the lungs leading to more severe lung pathology than seasonal H1N1, further suggesting that a higher pathogenic potential is associated with SOIV compared to other currently circulating H1N1 viruses (16, 17).

To better understand SOIV pathogenesis, we compared two genetically similar but clinically distinct Mexican isolates from the early stage of the pandemic in a macaque challenge model (18). We found that, in contrast to a current seasonal H1N1 virus, both SOIV isolates replicated in the upper and lower respiratory tract but differed in their clinical disease manifestation ranging from mild to severe pneumonia. The isolates showed striking heterogeneity in the extent of virus replication, host responses, and disease progression. This indicates concurrent circulation of strains with different pathogenic potential and thus explaining the distinct clinical picture for infected individuals.

## MATERIALS AND METHODS

**Viruses.** A/Mexico/4108/2009 (H1N1) (Mex4108) was isolated from a clinical specimen (kindly provided by the Centers for Disease Control and Prevention, Influenza Branch) obtained from a 4-year-old boy from Mexico who was mildly ill. A/Mexico/InDRE4487/2009 (H1N1) (Mex4487) was isolated from the bronchial aspirate of a 26-year-old man from a family cluster of three confirmed severe cases in Mexico (20). A/Kawasaki/UTK-4/2009 (H1N1) (Kaw) was isolated from a human and represents a recent seasonal virus (17). The viruses were grown in MDCK cells, harvested at a cytopathogenic effect of 3+ (>70% rounded off and detached cells) for virus stock preparation, and titrated by using a 50% tissue culture infective dose ($TCID_{50}$) assay on MDCK cells. The Mex4108, Mex4487, and Kaw infections were done with MDCK passage numbers 3, 2, and 2, respectively. All infectious work with the SOIVs was done under enhanced BSL3 conditions in the Integrated Research Facility of the Rocky Mountain Laboratories (RML), National Institute of Allergy and Infectious Disease (NIAID), National Institutes of Health (NIH).

***In vitro* infection (A549 cells).** Freshly seeded monolayer of A549 cells were infected with the different H1N1 virus isolates with $10^4$ $TCID_{50}$/100 μl/well. Following an adsorption of 1 h at 37°C, unbound viruses were washed away, and 1 ml of minimal essential medium (MEM) supplemented with 0.35 μg of TPCK (tolylsulfonyl phenylalanyl chloromethyl ketone)-trypsin/ml was added to the cultures. The cells were incubated at 37°C, and supernatants were collected at 12, 24, 48, and 72 h postinfection. Virus titration was performed by using a $TCID_{50}$ assay on MDCK cells.

***In vivo* infection (cynomolgus macaques).** Twenty-one cynomolgus macaques (*Macaca fascicularis*), 4 to 15 years old, weighing 3.0 to 8.7 kg, were evenly distributed with regard to age and weight over the different groups and infected with either Mex4108 ($n = 6$), Mex4487 ($n = 9$), or Kaw ($n = 6$) under anesthesia through a combination of intratracheal (4 ml), intranasal (0.5 ml per nostril), conjunctival (0.5 ml per eyelid), and oral (1 ml) routes with a suspension containing $10^6$ $TCID_{50}$/ml (the total infectious dose was $7 \times 10^6$ $TCID_{50}$) (18). The animals were monitored daily for clinical signs using an approved scoring sheet (fever, posture, respiration, feces/urine, food intake, recumbence, attitude, and skin turgor). On days −2, 0, 1, 3, 6, 8, 11, and 14 postinfection the animals were examined under anesthesia, at which point X-ray, pulse rate, blood pressure, temperature, and respiration rate were taken, and each animal was bled for blood chemistry analysis, differential blood count, virology, and cytokine profiles. Two (Mex4108) or three (Mex4487, Kaw) animals were euthanized and necropsied on days 1, 6, and 14 postinfection (Kaw only on days 1 and 6) with collection of clinical specimens from nasal mucosa, oral mucosa, conjunctiva, tonsils, cervical lymph nodes, trachea, bronchi, right and left lungs (upper, middle, and caudal), hilar lymph nodes, heart, liver, spleen, pancreas, jejunum, transverse colon, kidney, adrenal gland, and mesenteric lymph nodes. All animal experiments were approved by the RML Institutional Animal Care and Use Committee (IACUC) and performed according to the guidelines of the Association for Assessment and Accreditation of Laboratory Animal Care, International (AAALAC) by certified staff in an AAALAC-approved facility.

**Radiographic imaging and gross pathology scoring.** X-ray images were scored blindly according to the following scheme: grade 0, normal examination; grade 1, mild interstitial pulmonary infiltrates; grade 2, moderate interstitial pulmonary infiltrates, possibly including partial cardiac border effacement and small areas of pulmonary consolidation; and grade 3, pulmonary consolidation as primary lung pathology, often seen as progression from grade 2 lung pathology. The percentage of affected lung area was assessed in all lung lobes during necropsy by macroscopic examination.

**Hematology and serum biochemistry.** The total white blood cell (WBC) count, lymphocyte, platelet, reticulocyte, and red blood cell counts, hemoglobin, hematocrit values, mean cell volume, mean corpuscular volume, and mean corpuscular hemoglobin concentrations were determined from EDTA blood with the HemaVet 950FS+ laser-based hematology analyzer (Drew Scientific, Waterbury, CT). Plasma biochemistry was analyzed from heparin blood by using the blood chemistry analyzer iSTAT1 (Abbott Point of Care, Princeton, NJ). Urea nitrogen (BUN), glucose, chloride, sodium, potassium, hematocrit, hemoglobin, pH, $PCO_2$, $TCO_2$, base excess ($BE_{ecf}$), and anion gap values were determined by using an EC8+ cartridge. Creatinine values were evaluated by using Crea cartridges.

**Plasma cytokine analysis.** Concentrations of granulocyte colony-stimulating factor, granulocyte-macrophage colony-stimulating factor, gamma interferon, interleukin-1β (IL-1β), IL-4, IL-5, IL-6, IL-8, IL-17, monocyte chemotactic protein 1 (MCP-1), and macrophage inflammatory protein 1α in plasma of animals was determined on days 0, 1, 3, 6, 8, 11, and 14 postinfection by using a non-human primate cytokine Milliplex map kit (Millipore Corp., Billerica, MA) as described by the manufacturer. Samples were read by using a Bio-Plex 200 system (Bio-Rad, Hercules, CA).

**Virus titration.** Tissue samples were placed in RNAlater (Ambion) for subsequent RNA extraction (RNeasy kit; Qiagen). Tissue homogenates (10% [wt/vol]) were prepared in MEM-bovine serum albumin. Debris was pelleted by centrifugation ($2{,}000 \times g$, 5 min), and virus titers were determined in 10-fold dilutions of supernatant by standard $TCID_{50}$ assay on MDCK cells, in triplicate for each dilution. Virus titers were similarly determined in blood and swab suspensions.

**Histopathology and immunohistochemistry.** Animal tissues were fixed in 10% phosphate-buffered formalin. Fixed tissues were processed by conventional methods, embedded in paraffin, cut into 5-μm-thick sections, and stained with standard hematoxylin and eosin. Slides for immunohistochemistry were stained by using the Discovery XT and DAB map kit from Ventana Medical Systems (VMS), Tucson, AZ. The polyclonal SOIV (H1N1) hemagglutinin (HA) antibody (ProSci., Inc., Poway, CA) was diluted in antibody dilution buffer (VMS) at 1:500, followed by incubation for 32 min. Next, a biotinylated secondary of goat anti-rabbit SS Link (Biogenex, San Ramon, CA) was incubated for 32 min, followed by enzyme conjugate, and diaminobenzidine. Slides were counterstained with hematoxylin, dehydrated, cleared in xylene, and coverslipped.

**Microarray analysis.** Microarray analysis was performed using Agilent rhesus macaque 4×44K microarrays using the manufacturer's one-color analysis protocol. TaqMan was used to analyze lung samples for the presence of viral RNA. Because viral RNA was not detected in the sample available for microarray from animal 2 in the Mex4487 group, this animal was not included in subsequent transcriptional analyses. Gene expression in individual samples was quantified relative to gene expression from a pooled sample of lung RNA from seven uninfected cynomolgus macaques (five females and two males; ages, 7.5 to 12.9

years; 2.6 to 6.2 kg). Differential gene expression between the groups was identified at day 1 postinfection using a one-way Textbook analysis of variance (ANOVA; $P < 0.01$) using Rosetta Resolver (Rosetta Biosoftware). To filter gene sequence that changed minimally between treatment groups, gene sets from the ANOVAs were then filtered to include genes that changed as least 2-fold between any two of the treatment groups. Functional analysis of statistically significant gene expression changes was performed by using ingenuity pathway analysis (IPA; Ingenuity Systems), which analyzes gene expression data in the context of known biological response and regulatory networks. A Fisher exact test was used to determine the probability that each biological function assigned to that data set was due to chance alone. Heat maps for gene expression were created by using Spotfire DecisionSite 9.1.1. All gene expression data described here are publicly available at http://viromics.washington.edu.

## RESULTS AND DISCUSSION

**Selection and genetic characterization of SOIV strains.** To determine the virulence of the newly emerged SOIV in a recently established nonhuman primate model (18), we investigated two genetically similar but clinically distinct isolates from Mexico in comparison with the current seasonal H1N1 influenza virus strain A/Kawasaki/UTK-4/2009 (Kaw). A/Mexico/4108/2009 (Mex4108) and A/Mexico/InDRE4487/2009 (Mex4487) were isolated from human clinical specimens in the early stage of the pandemic. The two isolates from Mexico differed only in seven amino acid positions (PB2, amino acid [aa] 82; PA, aa 275, aa 581; HA aa 444; NP, aa 100, aa 373; and M2, aa 82) (see Table S1 in the supplemental material) but were isolated from cases with distinct clinical outcomes (Mex4108, mild single case; Mex4487, cluster of severe cases). In comparison to a hypothetical SOIV consensus sequence based on sequence data from early stage isolates of the pandemic, Mex4108 showed unique substitutions in the HA (aa 444), NP (aa 100), and M2 (aa 82) proteins, whereas Mex4487 had unique substitutions in the PB2 (aa 82) and PA (aa 275) proteins (see Table S1 in the supplemental material). None of the changes in these isolates, however, involves critical domains/motifs in PB1, PB2, HA, NA, and NS1 that have been implicated as influenza virulence markers (14, 19, 26, 27, 29, 33, 34), but all acquired the second-site suppressor mutation in PB2 (Q591R) that conveys enhanced polymerase activity in human cells (23).

**Clinical progression of SOIV infection.** Cynomolgus macaques were infected simultaneously via multiple routes (intratracheal, intranasal, ocular, and oral) with a total dose of $7 \times 10^6$ $TCID_{50}$ of either Kaw ($n = 6$), Mex4108 ($n = 6$), or Mex4487 ($n = 9$) using a protocol specifically optimized for infection with respiratory viruses of both the upper and the lower respiratory tracts (18). A similar challenge dose for all groups was confirmed by back titration of each inoculum on MDCK cells (Kaw, $1.1 \times 10^6$ $TCID_{50}$/ml; Mex4108, $1.1 \times 10^6$ $TCID_{50}$/ml; and Mex4487, $2 \times 10^6$ $TCID_{50}$/ml). Animals in the two SOIV-infected groups started to show signs of disease on days 1 to 2 postinfection with reduced food intake, slightly elevated temperature (≤2°F), and mild depression. In subsequent days, the animals exhibited reduced activity, piloerection, and signs of respiratory disease (e.g., increased respiration rate and nasal discharge) (Fig. 1A; see also Table S2 in the supplemental material). Clinical signs were generally milder and shorter-lived in Mex4108 compared to the moderate/severe and prolonged disease in Mex4487-infected animals. In contrast, cynomolgus macaques infected with the seasonal H1N1 virus (Kaw) showed either mild clinical signs or were clinically asymptomatic overall (Fig. 1A; see Table S2 in the supplemental material). Clinical manifestations and disease progression in Mex4487-infected animals were closer to those observed for infections with 1918 influenza viruses (same routes and similar dose), where animals showed very pronounced clinical symptoms early upon infection (days 1 to 2 postinfection) with rapid progression toward severe pneumonia or ARDS (5, 18). However, in contrast to 1918 virus-infected macaques, none of the SOIV-infected animals succumbed to the infection. Hematology showed elevated WBCs on day 1 postinfection for most animals, which was mainly due to increase in neutrophil numbers (data not shown). This most likely occurred as a result of infection and was not statistically significant among the different groups. All tested serum biochemistry parameters stayed within normal ranges.

Respiratory disease development was further examined by radiographic imaging (X-ray). The first signs of infiltration and interstitial markings were observed in the lungs of some SOIV-infected animals on day 1 postinfection. This developed into mild to moderate interstitial infiltrates and partial cardiac border effacement with small areas of pulmonary consolidation. Areas of pulmonary consolidation increased in density and distribution in the Mex4487-infected animals (Fig. 1B and 2C; see also Table S2 in the supplemental material). These animals were more severely affected compared to Mex4108-infected animals (Fig. 1B and 2B). Kaw-infected animals did not show any obvious X-ray abnormalities (Fig. 1B and 2A). Radiographic imaging was used to follow disease progression and allowed the detection of changes that peaked between days 6 and 8 postinfection for Mex4487 (Fig. 1B; see Table S2 in the supplemental material). In accordance with the severity of radiological changes, the respiration rate of the Mex4487-infected animals was significantly increased compared to the Kaw- and Mex4108-infected animals, which showed little to no X-ray abnormalities (Fig. 1C and 2; Table S2 in the supplemental material).

**Pathology and histopathology of SOIV infection.** Two (Mex4108) or three (Kaw and Mex4487) animals from each group were euthanized for necropsy on days 1, 6, and 14 postinfection (Kaw were only euthanized on days 1 and 6). Day 1 specimens were collected to study early disease progression and host immune responses. Day 6 postinfection was chosen for maximum pathology and day 14 was chosen to examine recovery from infection. We did not find clear evidence of virus-associated gross pathology in any of the groups 1 day after infection (Fig. 1D). The Kaw-infected group did not show any obvious gross pathology changes on either day 1 or 6 postinfection (Fig. 1D and 2A). In contrast, gross pathology was noted in both SOIV-infected groups on day 6 and was particularly pronounced in the animals infected with Mex4487, which developed more widely distributed and larger lung lesions (Fig. 1D; Fig. 2B and C). Specifically, affected lung lobes of animals infected with Mex4487 appeared dense with visible fluid exudates, indicating edema, and were plum colored and firm on palpation (Fig. 2C). Pulmonary lesions noted in animals infected with Mex4108 were characterized by multifocal, smaller, circumscribed, red areas and firm lung parenchyma (Fig. 2B). Mex4487-infected animals showed prolonged lung gross pathology at day 14 postinfection, a

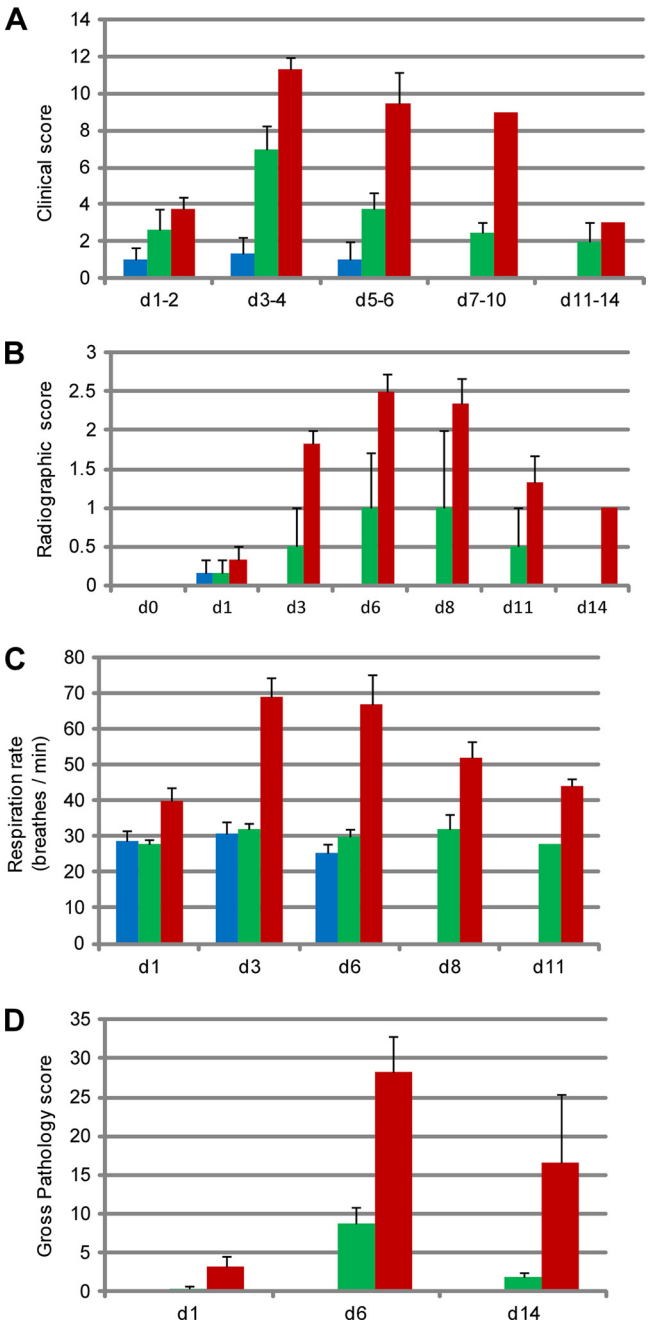


FIG. 1. Disease progression of infected cynomolgus macaques. Cynomolgus macaques were infected with a total dose of $7 \times 10^6$ $TCID_{50}$ of either Kaw (blue), Mex4108 (green), or Mex4487 (red) as described in Materials and Methods. (A) Clinical scoring. The scoring for clinical symptoms is described in Materials and Methods and in the legend to Table S2 in the supplemental material. Clinical scores were high and symptoms were prolonged in animals infected with Mex4487. The Mex4108-infected animals showed initial transient clinical symptoms, whereas the Kaw-infected animals were largely asymptomatic. (B) Radiographic scoring. The scoring for radiographic changes is described in Materials and Methods. The scores were higher for animals infected with Mex4487-infected animals compared to Mex4108- and Kaw-infected animals. Grading scheme: grade 0, normal examination; grade 1, mild interstitial pulmonary infiltrates; grade 2, moderate interstitial pulmonary infiltrates, may include partial cardiac border effacement, small areas of pulmonary consolidation; grade 3, pulmonary consolidation as primary lung pathology often seen as progression from grade 2 lung pathology. (C) Respiration rate. The respiration rate was determined during clinical examinations and is presented as breaths per minute. Respiration was increased for the Mex4487-infected animals only. (D) Gross pathology scoring. The lungs were visually inspected during necropsy and percentage scores (0 to 100%) for damage of lung tissue were assigned to the different lung lobes (upper, middle caudal). The average scores for both lungs are shown. Lung lesions peaked on day 6 postinfection and were highest for Mex4487-infected animals. A notable degree of lesion area in lungs of the Mex4487-infected animals was observed on day 14 postinfection. Error bars represent the standard errors of the mean.

finding suggestive of extended virus replication in Mex4487-infected animals (Fig. 1D).

Histologic changes on day 1 postinfection in lungs from the SOIV-infected animals were comparable and interpreted as multifocal, minimal to moderate, acute pneumonia characterized by alveolar and bronchiolar infiltrates of mostly neutrophils, fewer macrophages, few lymphocytes, and variable amounts of hemorrhage (Fig. 3C and E). Multifocal, mild alveolar and bronchiolar edema, occasional alveolar fibrin, multifocal degeneration and necrosis of bronchiolar epithelium, and multifocal perivascular lymphocytic infiltrates were also noted (Fig. 3C and E). In contrast, changes in the lungs from Kaw-infected animals were primarily characterized by minimally increased numbers of neutrophils in alveolar septae and mild alveolar histiocytosis with multifocal, mild lymphohistiocytic perivasculitis, and, occasionally, low numbers of neutrophils and macrophages within the lumen of bronchioles (Fig. 3A). Immunohistochemical (IHC) staining for viral HA antigen of SOIV-infected lungs on day 1 postinfection revealed moderately abundant antigen positivity in alveolar epithelium and less frequent staining of bronchiolar epithelium. HA-specific staining was also observed in alveolar luminal cells, which were interpreted as sloughed alveolar epithelial cells, alveolar macrophages, or both (Fig. 3D and F). In contrast, only rare, single alveolar epithelial cells and macrophages were viral antigen positive in lung samples from Kaw-infected animals on day 1 postinfection (Fig. 3B).

Lung histopathology from SOIV-infected animals necropsied on day 6 postinfection were similar and interpreted as mild to severe subacute to chronic pneumonia characterized by alveolar edema, fibrin, extensive type II alveolar pneumocyte hyperplasia and occasional hyaline membrane formation (Fig. 3I and K). There were numerous macrophages, neutrophils, and lymphocytes, with variable amounts of edema and fibrin within alveolar and bronchiolar lumina, and alveolar septae were expanded by similar inflammatory components. Multifocal perivascular lymphohistiocytic and eosinophilic inflammation was also noted (Fig. 3I and K). In contrast, only minimal alveolar and bronchiolar inflammation was noted in lungs from the Kaw group necropsied at day 6 postinfection (Fig. 3G). Histopathological changes were characterized by multifocal, mild accumulations of macrophages with microvesicular, foamy cytoplasm within alveoli and bronchiolar lumina, and multifocal perivascular infiltrates of lymphocytes and macrophages (Fig. 3G). IHC staining of lung tissue for the presence of HA antigen on day 6 postinfection was comparable in the Kaw- and Mex4108-infected animals (Fig. 3H and J) with only

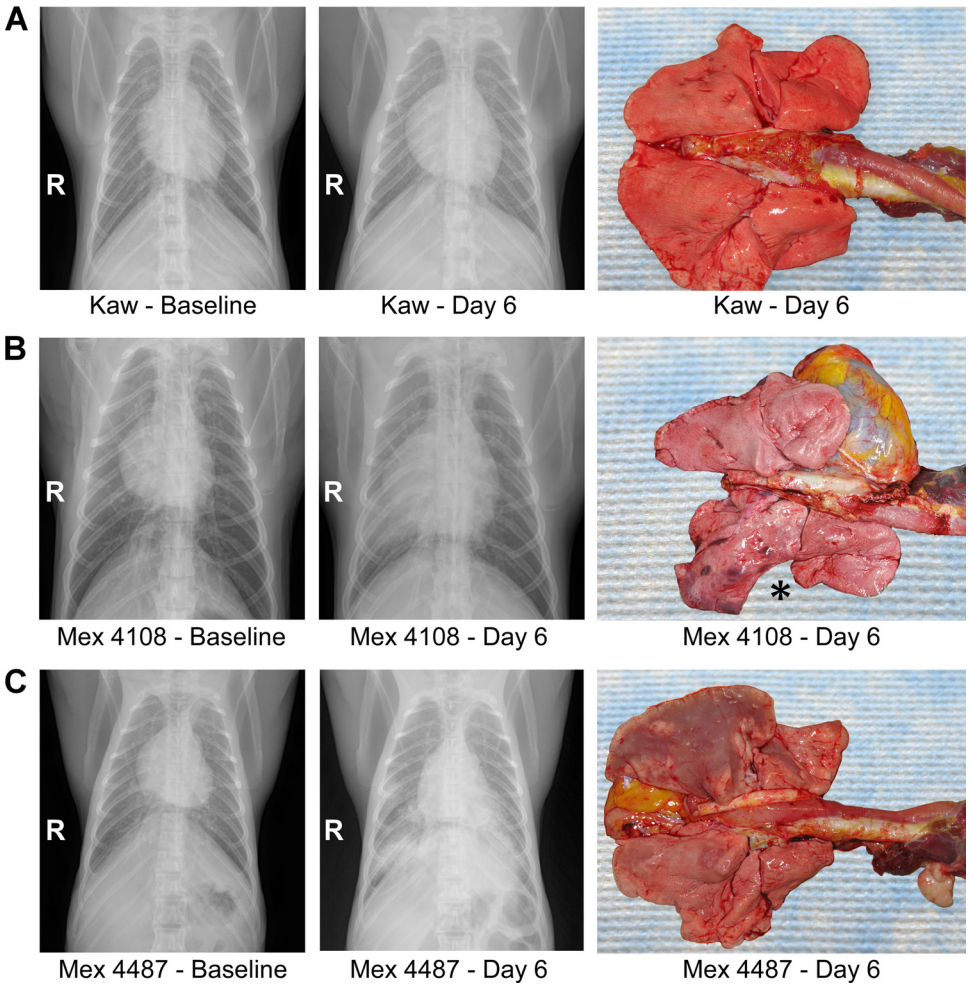


FIG. 2. Radiological and gross pathological examination of the lungs of infected cynomolgus macaques. Cynomolgus macaques were infected as described in Materials and Methods with a total dose of $7 \times 10^6$ $TCID_{50}$ of either Kaw (A), Mex4108 (B), or Mex4487 (C). The radiographic images (X-ray) shown are of a representative animal from each group. Images were taken from the same animal at day 1, prior to infection, and at day 6 postinfection (postmortem). Extensive lung infiltrations were seen on day 6 X-ray image for Mex4487, whereas Mex4108 and Kaw showed little to no infiltrations. Accordingly, extensive lesions were visible in the lungs of the animals infected with Mex4487 on day 6 postinfection. The asterisk (*) indicates a localized lesion in the caudal right lobe of a Mex4108-infected animal.

rare staining of macrophages and alveolar epithelial cells. Antigen-positive cells were notable and observed more frequently in the Mex4487-infected lung sections at day 6 postinfection (Fig. 3L), indicating prolonged replication of this isolate in lung tissue, as was suggested by the presence of gross pathology lesions (Fig. 1D). By day 14 postinfection, small clusters of antigen positive cells were observed, though rarely, in the Mex4487-infected lung sections, but not in the Mex4108-infected sections (data not shown). Overall, the histopathological features described here are comparable with influenza virus infections in humans (11, 21, 38) and have been reported in animal models of severe acute respiratory syndrome coronavirus (32).

Overall, lung pathology was different between the two SOIV isolates with multifocal small versus large pronounced and widely distributed affected areas in Mex4108- and Mex4487-infected animals, respectively (Fig. 1D; Fig. 2B and C). However, lung histopathology of selected affected areas did not reveal major differences between the two SIOV isolates (Fig. 3). In contrast, Kaw-infected animals showed nearly no gross lung pathology and histopathological changes were focal and less pronounced (Fig. 1D, Fig. 2, and Fig. 3).

**Extent of SOIV replication.** All three viruses (Kaw, Mex4108, and Mex4487) were detected to similar high titers in upper and lower respiratory tract tissues on day 1 postinfection (Fig. 4A). Sustained replication in lower respiratory tract tissue could only be found with Mex4487, with similar titers on days 1 and 6 postinfection (Fig. 4A and B). There was no evidence for systemic spread of any of the viruses as indicated by the absence of viremia and nondetectable virus titers in other selected organs (for a list of tested organs, see Materials and Methods).

*In vitro* growth in human lung carcinoma cells (A549) showed similar growth kinetics within the first 48 h for both SOIVs and Kaw, supporting *in vivo* data obtained on day 1 postinfection (Fig. 4A and C). In contrast, later in infection (day 3 postinfection), Mex4487 showed an *in vitro* replication advantage with titers >1 log higher compared to Mex4108 and

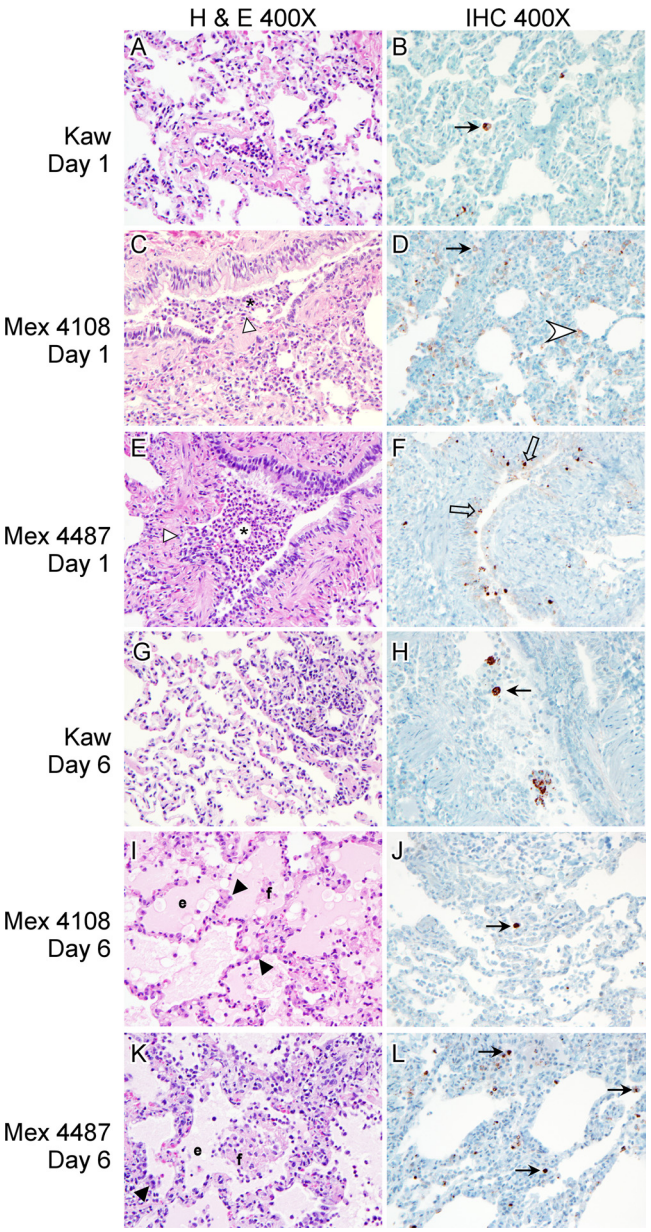


FIG. 3. Histological examination of lungs of infected cynomolgus macaques. Cynomolgus macaques were infected as described in Materials and Methods, with a total dose of $7 \times 10^6$ $TCID_{50}$ of either Kaw, Mex4108, or Mex4487. Hematoxylin and eosin (H&E) and immunohistochemistry (IHC; anti-HA antigen)-stained sections of lungs from cynomolgus macaques necropsied at day 1 postinfection (A to F) and day 6 postinfection (G to L) are shown. At day 1 postinfection, there was neutrophilic exudate within the lumen of bronchioles and necrosis and loss of bronchiolar epithelium in the lungs of SOIV-infected animals (* and open arrowhead, respectively, panels C and E) and only minimal inflammation noted in Kaw-infected lungs (A). At day 6 postinfection, there was extensive alveolar edema, fibrin and type II alveolar pneumocyte hyperplasia in the lungs of SOIV-infected animals (e and f, arrowhead, respectively, panels I and K). IHC (anti-HA antigen) is demonstrated in alveolar epithelial cells (white arrowhead), bronchiolar epithelial cells (open arrow), and macrophages (black arrow) (B, D, F, H, J, and L).

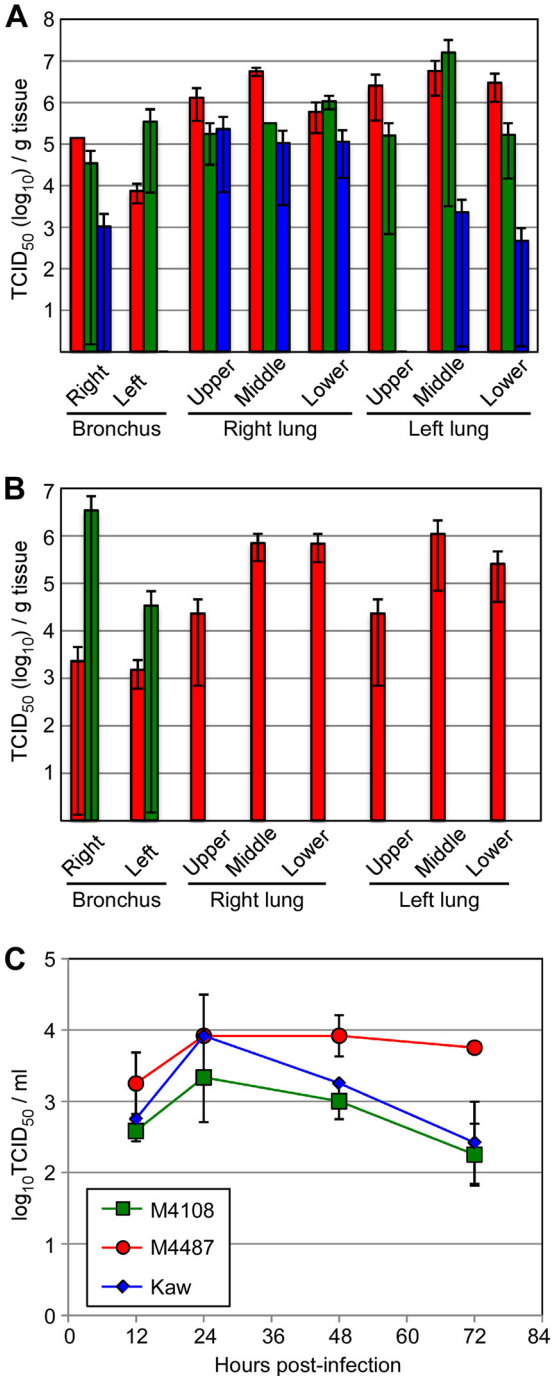


FIG. 4. Virus replication in the upper and lower respiratory tracts as well as tissue culture. Cynomolgus macaques were infected as described in Materials and Methods with a total dose of $7 \times 10^6$ $TCID_{50}$ of either Kaw (blue), Mex4108 (green), or Mex4487 (red). Virus titers were determined by $TCID_{50}$ assay from tissue specimens collected during necropsies on day 1 (A) and 6 (B) postinfection. (C) Growth kinetics of the different viruses in A549 cells over 72 h. Error bars represent the standard errors of the mean.

Kaw (Fig. 4C), consistent with the prolonged *in vivo* replication of this isolate in lung tissue (Fig. 4B).

We further analyzed infectivity of mucosal membranes as an indicator for virus shedding and a potential marker for trans-

mission. Throughout the experiment oral and rectal swabs remained negative for infectious virus (data not shown). Virus detection in nasal swabs was inconsistent and ranged from 0 to 50% of the infected animals being positive in each group. Interestingly, with some Mex4108-infected animals virus could be detected in nasal swabs for up to day 8 postinfection, whereas virus seemed to be cleared from Mex4487- and Kaw-infected animals by day 6 (data not shown). Further studies are needed to address this important epidemiological marker of SOIVs and its implication for public health, but the preliminary data here might suggest a potential difference in transmissibility among SOIV isolates. In that regard, two previous transmissibility studies in ferrets reported contradictory results, with one group reporting similar transmissibility (24) and the other reporting a less efficient transmissibility (22) when comparing a single SOIV isolate with seasonal H1N1 viruses.

**Host transcriptional responses to SOIV infection.** To explore the early transcriptional responses to infection with the two SOIV isolates, we performed microarray analysis on lung samples taken at necropsy on day 1 postinfection. ANOVA revealed 788 gene expression differences that distinguished the isolates (Fig. 5; see Table S3 in the supplemental material). The greatest number of expression differences was between Kaw and Mex4487, whereas differences between the SOIV-infected animals were more subtle (see Table S4 in the supplemental material). IPA was used to evaluate the biological pathways associated with these differences in transcription. Inflammatory response was among the top biological categories of genes that distinguished the groups at day 1 postinfection (Fig. 6A; see Table S5 in the supplemental material). The inflammatory response genes represented were most significantly related to immune response, cell activation, cell movement, and phagocytosis, with many of the genes within this category playing roles in more than one biological function. Examination of expression patterns of these genes suggested the most robust induction of genes within the Mex4487-infected animals, with the Mex4108 strain exhibiting an intermediate expression phenotype between those of Mex4487 and Kaw. In contrast, a decrease in expression was observed for many of these genes in the Kaw animals. Intracellular NF-κB signaling molecules were upregulated to the greatest extent in the Mex4487-infected animals (Fig. 6B). This upregulation was concurrent with a robust induction of directly related cytokine/chemokine and antigen presentation molecules. These differences in response were less pronounced in the Mex4108-infected animals and relatively rare in the Kaw-infected animals. Given the similarities in virus titer in the lung at day 1 postinfection (Fig. 4), these differences in host response cannot be attributed solely to viral levels in the lung. The greater expression of genes in response to the SOIV strains compared to the Kaw isolate is in agreement with the greater infiltration of immune cells into the lung at day 1 postinfection (Fig. 3) and is predictive of the greater tissue damage observed in the lungs at day 6 postinfection (Fig. 1D and 2).

**Proinflammatory cytokine levels after SOIV infection.** To further investigate the differences in inflammation noted in the transcriptional data, we analyzed the levels of selected inflammatory mediators in the blood of SOIV-infected animals. We observed increased, early systemic inflammatory responses following infection with the Mex4487 strain that was less pronounced in animals infected with Mex4108 or Kaw isolates. In particular, plasma cytokine analysis revealed the greatest increase in the levels of IL-6 and MCP-1 in the Mex4487-infected animals early after infection (Fig. 7). The increased levels of proinflammatory plasma cytokines were in accord with the increase in inflammatory gene expression observed in the lungs of SOIV-infected animals at day 1 postinfection compared to Kaw-infected animals (Fig. 5; see Table S6 in the supplemental material). In particular, greater IL-6 gene expression was also observed in the lungs of Mex4487-infected animals on day 1 postinfection, with intermediate and low levels for the Mex4108- and Kaw-infected groups, respectively. The trends observed for IL-6 gene expression in the lungs were similar to expression patterns for the proinflammatory cytokines TNF-α and IL-1β (see Table S6 in the supplemental material). Severe influenza virus infection is associated with increased early and prolonged inflammatory responses (7, 8, 18), and increased protein levels of IL-6 have also been reported in response to infection with more virulent H1N1 strains in ferrets (37), severe 1918 infections in macaques (18),

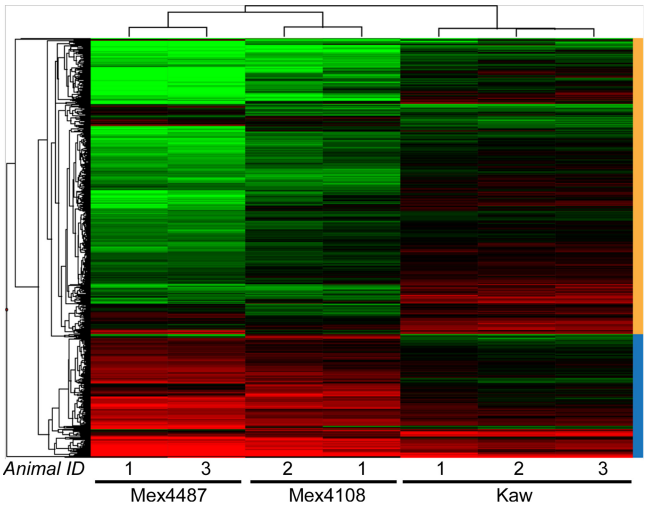


FIG. 5. Differential host transcriptional responses. Cynomolgus macaques were infected as described in Materials and Methods with a total dose of $7 \times 10^6$ $TCID_{50}$ of either Kaw, Mex4108, or Mex4487. The animals were euthanized on day 1 postinfection, and the total RNA was isolated from lung tissue. The figure shows one-dimensional clustering of genes with statistically different expression in the lung at day 1 postinfection (788 gene sequences; see Table S3 in the supplemental material) as determined by one-way ANOVA ($P \leq 0.05$, selecting for sequences that were 2-fold different between at least two of the treatments). Clustering of expression data for each animal was performed by using hierarchical unweighted pair-group method with arithmetic mean (UPGMA) with Euclidean distance similarity measure using an average value ordering function. The dendrogram at the top of the heat map indicates the overall similarities in gene expression between the individual animals. The dendrogram on the left side of the heat map indicates the similarities in expression between the differentially expressed genes. On the right side of the heat map, two major groups are indicated in orange (563 gene sequences) and blue (225 gene sequences). Gene expression for an animal is shown as the log(ratio) of expression relative to a common reference pool of RNA extracted from lungs of uninfected cynomolgus macaques. Red indicates that the gene expression is higher than the uninfected reference; green indicates that gene expression is lower than the uninfected reference sample.

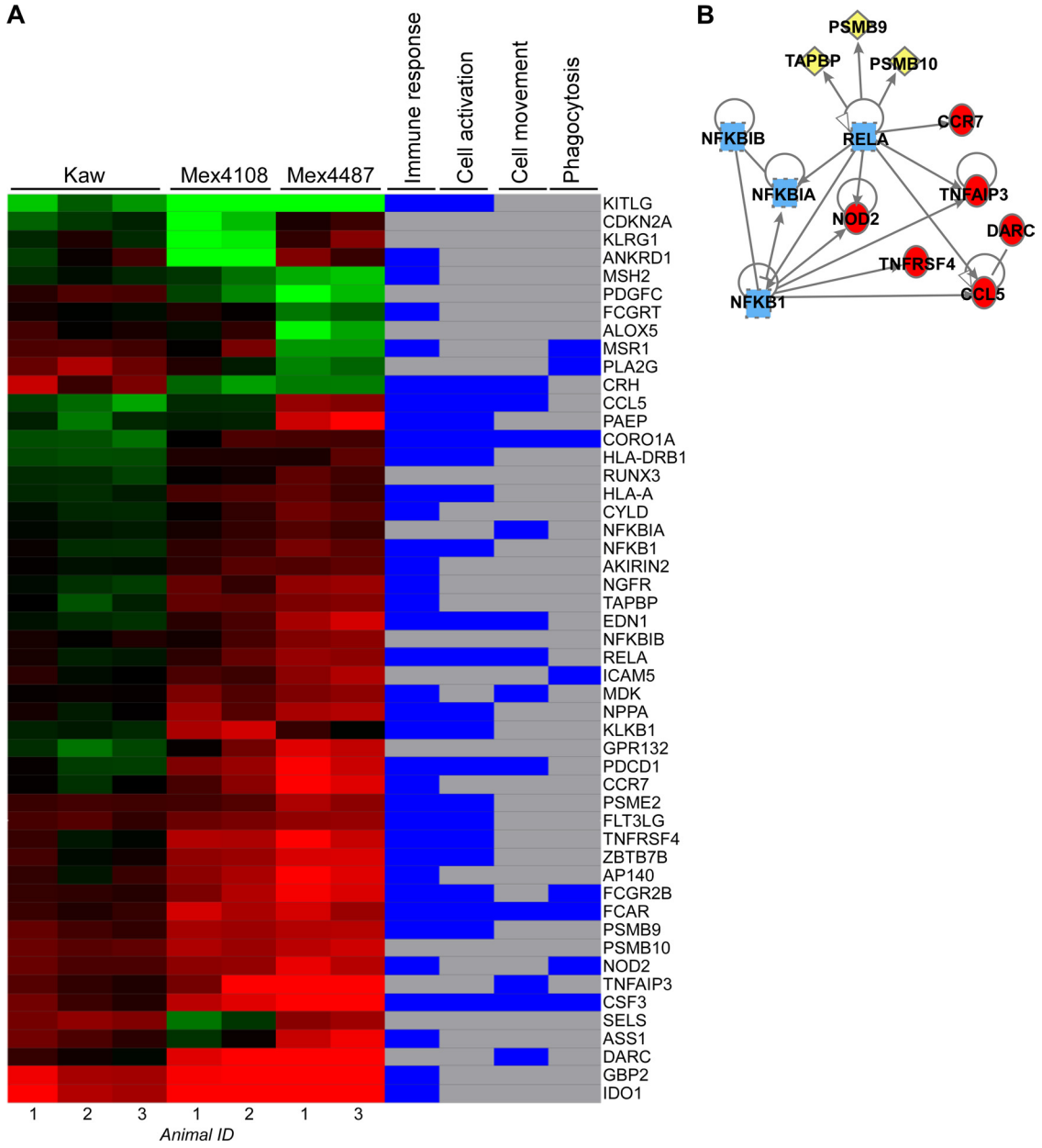


FIG. 6. Differential host transcriptional responses of inflammatory response-related genes. (A) One-dimensional clustering of genes in relation to inflammatory response. The average expression for each animal is shown as the log(ratio) of expression relative to a common reference pool of RNA extracted from lungs of uninfected cynomolgus macaques. Red indicates that the gene expression is higher than the uninfected reference; green indicates that gene expression is lower than uninfected reference sample. Clustering of expression data for each animal was performed by using hierarchical UPGMA with a Euclidean distance similarity measure using an average value ordering function. The association of each molecule within the biological pathways (right) is shown, with blue denoting an association with the pathway and gray denoting no association with the select pathway. (B) Network diagram depicting the relationship between NF-κB signaling molecules (shown in light blue), antigen presentation (shown in yellow), and cytokine/chemokine-related molecules (shown in red). Molecules in the network were selected from differentially regulated inflammatory response genes based on their direct interactions with each other, as determined by functional analysis performed using IPA (Ingenuity Systems).

and a fatal human case of SOIV (25), but not from infections with contemporary H1N1 viruses in macaques (18). IL-6 levels have also been associated with mediating the clinical manifestation of influenza virus infections in humans (15, 35), and thus may be an indicator for progression to more severe disease caused by influenza viruses.

The plasma levels of MCP-1 were significantly higher in Mex4487-infected animals on day 1 postinfection compared to those observed in Mex4108- and Kaw-infected animals (Fig. 7). Gene expression of MCP-1 was upregulated in the lungs at day 1 postinfection in all groups, with the greatest transcriptional response in animals infected with Mex4487. Elevated MCP-1 levels were also found in sera of 1918 virus-infected macaques (18) and the sera and lung tissues of a fatal human SOIV case

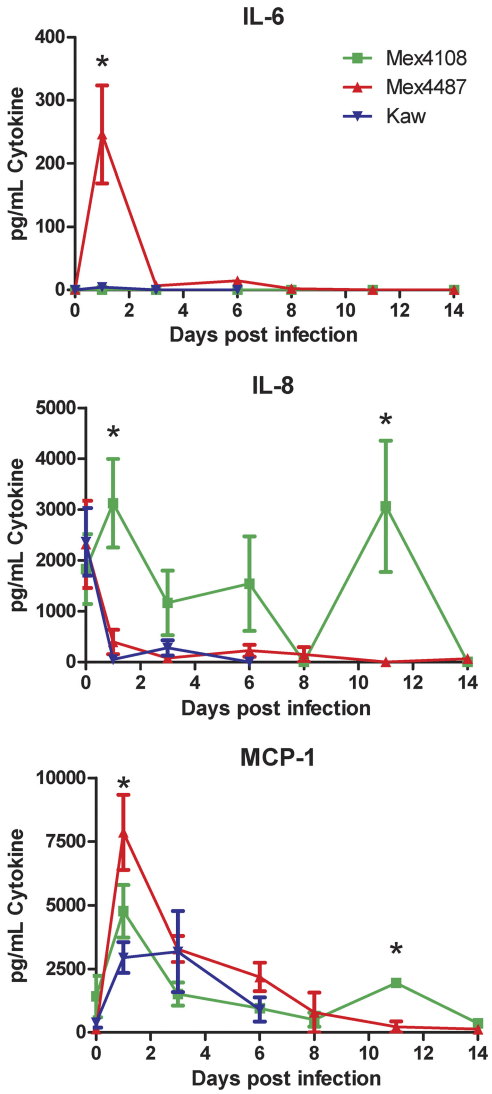


FIG. 7. Cytokine responses in plasma of infected cynomolgus macaques. Cynomolgus macaques were infected as described in Materials and Methods with a total dose of $7 \times 10^6$ $TCID_{50}$ of either Kaw (blue), Mex4108 (green), or Mex4487 (red). Animals were bled on 1, 3, 6, 8, 11, and 14 days postinfection, and cytokine levels in plasma were analyzed by a bioplex assay. We show here the concentrations for IL-6 (upper graph), IL-8 (middle graph), and MCP-1 (lower graph). Mean cytokine concentrations are expressed as pg/ml. Error bars represent the standard errors of mean. The asterisks represent significant differences compared to the Kaw group by using two-way ANOVA ($P < 0.05$).

(25). In contrast, IL-8 responses were significantly higher in Mex4108-infected animals, similar to ferrets infected with less-virulent H1N1 viruses (37). Overall, the induction of the proinflammatory response was not as pronounced with Mex4108 and the seasonal Kaw virus, which behaved similarly to what was described previously for the seasonal human A/Kawasaki/173/01 (H1N1) (18) and A/Texas/36/91 (H1N1) (2, 4) isolates.

**Conclusions.** The two SOIV isolates caused mild to severe pneumonia in the cynomolgus macaque model demonstrating a higher virulence than the seasonal H1N1 isolate (Kaw). Clinical signs following SOIV infection ranged from mild to severe and were more advanced over the relatively mild infections caused by seasonal influenza viruses such as Kaw (Fig. 1A; see Table S2 in the supplemental material), A/Kawasaki/173/01 (H1N1), and A/Texas/36/91 (H1N1) (2, 4, 18). Pathological and radiological changes observed with the SOIV isolates were in accordance with moderate to severe interstitial pneumonia (Fig. 2 and 3) and were also more severe than those observed with the above-mentioned seasonal influenza virus strains (2, 4, 18). Overall, these findings assign the newly emerged SOIV isolates to an intermediate virulence phenotype in macaques between seasonal influenza and the more severe infections caused by the highly virulent H5N1 (5, 31) and 1918 H1N1 (18) viruses.

The striking heterogeneity in virulence in the cynomolgus macaque model between SOIV isolates is particularly interesting given that the isolates are two genetically similar strains and are derived from the same geographical region during the early stage of the pandemic. The Mex4487 isolates caused more severe pneumonia with prolonged replication in the lower respiratory tract (Fig. 1 to 4; see Table S2 in the supplemental material). This differs from contemporary seasonal human H1N1 influenza virus strains that are characterized in this animal model by a short-term virus presence, mainly in the upper respiratory tract (2, 4, 18, 38) or, if inoculated intratracheally, by rapid clearance from lung tissue (Fig. 4A and B). This observation could be due in part to differences in virus replication as Mex4487 replicated to higher titers and over a prolonged period in human lung carcinoma cells (A549) (Fig. 4C). Some distinct features of individual SOIV isolates observed in the present study might be controlled by differences in *in vivo* replication and/or host responses which could be associated with certain amino acid substitutions (see Table S1 in the supplemental material). However, no distinct molecular motifs have been described for SOIV H1N1 isolates, in contrast to the virulence markers identified in H5N1 and 1918 H1N1 viruses (14, 19, 26, 27, 29, 33, 34). We have started to analyze the impact of the mutations found between the Mex4108 and Mex4487 strains (see Table S1 in the supplemental material) using reverse genetics. It will be critical to identify molecular fingerprints associated with a pathogenic phenotype to support future patient management and public health responses.

## ACKNOWLEDGMENTS

We thank Edward Schreckendgust, Rocky Rivera, Sandy Skorupa, and Kathleen Meuchel (Division of Intramural Research, NIAID, NIH) for assistance in animal care and basic animal procedures and Anita Mora, Austin Athman, and Gary Hettrick (Division of Intramural Research, NIAID, NIH) for their assistance with graphical work. We further acknowledge Victoria Carter, Elizabeth Rosenzweig, and Lauri Aicher (University of Washington) for microarray technical assistance. We are grateful to TIB Molbiol, Adelphia, NJ, for providing the oligonucleotides used in this study.

The study was financially supported by the Division of Intramural Research, National Institute of Allergy and Infectious Diseases, National Institutes of Health; Public Health Service grants P51RR000166 and R24RR016354 and NIAID contract HHSN272200800060C awarded to M.G.K.; The Public Health Agency of Canada and the Team Grant 310641 awarded to D.K., H.F., and G.K.; and by Grants-in-Aid for Specially Promoted Research and for Scientific Research, by a Contract Research Fund for the Program of Founding Research Centers for Emerging and Reemerging Infectious Diseases, by ERATO (Japan Science and Technology Agency), by the Special Co-

ordination Funds for Promoting Science and Technology from the Ministry of Education, Culture, Sports, Science, and Technology of Japan, by National Institute of Allergy and Infectious Diseases Public Health Service research grants, and by an NIAID-funded Center for Research on Influenza Pathogenesis (CRIP, HHSN266200700010C), all awarded to Y.K.

## REFERENCES


1. **Anonymous.** 2009. Pandemic alert level 6: sustained community transmission of influenza A (H1N1) virus in two different WHO regions. Eur. Surveill. **14:**19237.
2. **Baas, T., et al.** 2006. Integrated molecular signature of disease: analysis of influenza virus-infected macaques through functional genomics and proteomics. J. Virol. **80:**10813–10828.
3. **Barnard, D. L.** 2009. Animal models for the study of influenza pathogenesis and therapy. Antivir. Res. **82:**A110–A122.
4. **Baskin, C. R., et al.** 2007. Functional genomic and serological analysis of the protective immune response resulting from vaccination of macaques with an NS1-truncated influenza virus. J. Virol. **81:**11817–11827.
5. **Baskin, C. R., et al.** 2009. Early and sustained innate immune response defines pathology and death in nonhuman primates infected by highly pathogenic influenza virus. Proc. Natl. Acad. Sci. U. S. A. **106:**3455–3460.
6. **Chowell, G., et al.** 2009. Severe respiratory disease concurrent with the circulation of H1N1 influenza. N. Engl. J. Med. **361:**674–679.
7. **Cilloniz, C., et al.** 2009. Lethal influenza virus infection in macaques is associated with early dysregulation of inflammatory related genes. PLoS Pathog. **5:**e1000604.
8. **de Jong, M. D., et al.** 2006. Fatal outcome of human influenza A (H5N1) is associated with high viral load and hypercytokinemia. Nat. Med. **12:**1203–1207.
9. **Fraser, C., et al.** 2009. Pandemic potential of a strain of influenza A (H1N1): early findings. Science **324:**1557–1561.
10. **Garten, R., et al.** 2009. Antigenic and genetic characteristics of swine-origin 2009 A (H1N1) influenza viruses circulating in humans. Science **325:**197–201.
11. **Gill, J. R., et al.** 2010. Pulmonary pathologic findings of fatal 2009 pandemic influenza A/H1N1 viral infections. Arch. Pathol. Lab. Med. **134:**235–243.
12. **Ginsberg, M., et al.** 2009. Swine influenza A (H1N1) infection in two children–Southern California, March-April 2009. MMWR Morb. Mortal. Wkly. Rep. **58:**400–401.
13. **Hartley, C. A., P. C. Reading, A. C. Ward, and E. M. Anders.** 1997. Changes in the hemagglutinin molecule of influenza type A (H3N2) virus associated with increased virulence for mice. Arch. Virol. **142:**75–88.
14. **Hatta, M., P. Gao, P. Halfmann, and Y. Kawaoka.** 2001. Molecular basis for high virulence of Hong Kong H5N1 influenza A viruses. Science **293:**1840–1842.
15. **Hayden, F. G., et al.** 1998. Local and systemic cytokine responses during experimental human influenza A virus infection: relation to symptom formation and host defense. J. Clin. Invest. **101:**643–649.
16. **Herfst, S., et al.** 2010. Pandemic 2009 H1N1 influenza virus causes diffuse alveolar damage in cynomolgus macaques. Vet. Pathol. doi:10.1177/0300985810374836.
17. **Itoh, Y., et al.** 2009. In vitro and in vivo characterization of new swine-origin H1N1 influenza viruses. Nature **460:**1021–1025.
18. **Kobasa, D., et al.** 2007. Aberrant innate immune response in lethal infection of macaques with the 1918 influenza virus. Nature **445:**319–323.
19. **Kobasa, D., et al.** 2004. Enhanced virulence of influenza A viruses with the haemagglutinin of the 1918 pandemic virus. Nature **431:**703–707.
20. **Kobinger, G. P., et al.** 2010. Assessment of the efficacy of commercially available and candidate vaccines against a pandemic H1N1 2009 virus. J. Infect. Dis. **201:**1000–1006.
21. **Kuiken, T., and J. K. Taubenberger.** 2008. The pathology of human influenza revisited. Vaccine **26**(Suppl. 4)**:**D59–D66.
22. **Maines, T. R., et al.** 2009. Transmission and pathogenesis of swine-origin 2009 A (H1N1) influenza virus in ferrets and mice. Science **325:**484–487.
23. **Mehle, A., and J. A. Doudna.** 2009. Adaptive strategies of the influenza virus polymerase for replication in humans. Proc. Natl. Acad. Sci. U. S. A. **106:**21312–21316.
24. **Munster, V. J., et al.** 2009. Pathogenesis and transmission of swine-origin 2009 A (H1N1) influenza virus in ferrets. Science **325:**481–483.
25. **Nakajima, N., et al.** 2010. The first autopsy case of pandemic influenza (A/H1N1pdm) virus infection in Japan: detection of a high copy number of the virus in type II alveolar epithelial cells by pathological and virological examination. Jpn. J. Infect. Dis. **63:**67–71.
26. **Neumann, G., and Y. Kawaoka.** 2006. Host range restriction and pathogenicity in the context of influenza pandemic. Emerg. Infect. Dis. **12:**881–886.
27. **Neumann, G., T. Noda, and Y. Kawaoka.** 2009. Emergence and pandemic potential of swine-origin H1N1 influenza virus. Nature **459:**931–939.
28. **Novel Swine-Origin Influenza A (H1N1) Virus Investigation Team.** 2009. Emergence of a novel swine-origin influenza A (H1N1) virus in humans. N. Engl. J. Med. **360:**2605–2615.
29. **Pappas, C., et al.** 2008. Single gene reassortants identify a critical role for PB1, HA, and NA in the high virulence of the 1918 pandemic influenza virus. Proc. Natl. Acad. Sci. U. S. A. **105:**3064–3069.
30. **Perez-Padilla, R., et al.** 2009. Pneumonia and respiratory failure from swine-origin influenza A (H1N1) in Mexico. N. Engl. J. Med. **361:**680–689.
31. **Rimmelzwaan, G. F., et al.** 2001. Pathogenesis of influenza A (H5N1) virus infection in a primate model. J. Virol. **75:**6687–6691.
32. **Rockx, B., et al.** 2007. Synthetic reconstruction of zoonotic and early human severe acute respiratory syndrome coronavirus isolates that produce fatal disease in aged mice. J. Virol. **81:**7410–7423.
33. **Salomon, R., et al.** 2006. The polymerase complex genes contribute to the high virulence of the human H5N1 influenza virus isolate A/Vietnam/1203/04. J. Exp. Med. **203:**689–697.
34. **Seo, S. H., E. Hoffmann, and R. G. Webster.** 2002. Lethal H5N1 influenza viruses escape host antiviral cytokine responses. Nat. Med. **8:**950–954.
35. **Skoner, D. P., D. A. Gentile, A. Patel, and W. J. Doyle.** 1999. Evidence for cytokine mediation of disease expression in adults experimentally infected with influenza A virus. J. Infect. Dis. **180:**10–14.
36. **Smith, G. J., et al.** 2009. Origins and evolutionary genomics of the 2009 swine-origin H1N1 influenza A epidemic. Nature **459:**1122–1125.
37. **Svitek, N., P. A. Rudd, K. Obojes, S. Pillet, and V. von Messling.** 2008. Severe seasonal influenza in ferrets correlates with reduced interferon and increased IL-6 induction. Virology **376:**53–59.
38. **Taubenberger, J. K., and D. M. Morens.** 2008. The pathology of influenza virus infections. Annu. Rev. Pathol. **3:**499–522.